RADIATION RESEARCH **179**, 690–697 (2013)
0033-7587/13 $15.00

DOI: 10.1667/R3043.1

Integration of Monte Carlo Simulations with PFGE Experimental Data Yields Constant RBE of 2.3 for DNA Double-Strand Break Induction by Nitrogen Ions between 125 and 225 keV/μm LET

D. Alloni,[a,b,c] A. Campa,[d,e,1] W. Friedland,[f] L. Mariotti[b,c] and A. Ottolenghi[b,c]

[a] *Laboratory of Applied Nuclear Energy, Università degli studi di Pavia, Italy;* [b] *Physics Department, Università degli studi di Pavia, Italy;* [c] *National Institute of Nuclear Physics (INFN), Sezione di Pavia, Italy;* [d] *Health and Technology Department, Istituto Superiore di Sanità, Roma, Italy;* [e] *National Institute of Nuclear Physics (INFN), Sezione di Roma1, Gruppo Collegato Sanità, Roma, Italy; and* [f] *Helmholtz Zentrum München, Institute of Radiation Protection, Neuherberg, Germany*

Alloni, D., Campa, A., Friedland, W., Mariotti, L. and Ottolenghi, A. Integration of Monte Carlo Simulations with PFGE Experimental Data Yields Constant RBE of 2.3 for DNA Double-Strand Break Induction by Nitrogen Ions between 125 and 225 keV/μm LET. *Radiat. Res*. 179, 690–697 (2013).

The number of small radiation-induced DNA fragments can be heavily underestimated when determined from measurements of DNA mass fractions by gel electrophoresis, leading to a consequent underestimation of the initial DNA damage induction. In this study we reanalyzed the experimental results for DNA fragmentation and DNA double-strand break (DSB) yields in human fibroblasts irradiated with γ rays and nitrogen ion beams with linear energy transfer (LET) equal to 80, 125, 175 and 225 keV/μm, originally measured by Höglund *et al*. (*Radiat Res* 155, 818–825, 2001 and *Int J Radiat Biol* 76, 539–547, 2000). In that study the authors converted the measured distributions of fragment masses into DNA fragment distributions using mid-range values of the measured fragment length intervals, in particular they assumed fragments with lengths in the interval of 0–48 kbp had the mid-range value of 24 kbp. However, our recent detailed simulations with the Monte Carlo code PARTRAC, while reasonably in agreement with the mass distributions, indicate significantly increased yields of very short fragments by high-LET radiation, so that the actual average fragment lengths, in the interval 0–48 kbp, 2.4 kbp for 225 keV/μm nitrogen ions were much shorter than the assumed mid-range value of 24 kbp. When the measured distributions of fragment masses are converted into fragment distributions using the average fragment lengths calculated by PARTRAC, significantly higher yields of DSB related to short fragments were obtained and resulted in a constant relative biological effectiveness (RBE) for DSB induction yield of 2.3 for nitrogen ions at 125–225 keV/μm LET. The previously reported downward trend of the RBE values over this LET range for DSB induction appears to be an artifact of an inadequate average fragment length in the smallest interval.

[1]Address for correspondence: Health and Technology Department, Istituto Superiore di Sanità, Viale Regina Elena 299, 00161 Roma, Italy; e-mail: campa@iss.infn.it.

INTRODUCTION

The cellular effects induced by different radiation qualities have been studied intensively [e.g., refs. (*1–8*)] and numerous studies, both experimental and theoretical, have investigated the different patterns of DNA damage, in particular radiation induced DNA double-strand breaks (DSBs), caused by different ionizing radiations (*9–24*). In the past, the experimental determination of DNA fragmentation spectra was mainly performed by gel electrophoresis (*13, 21, 22*). These measurements found only a mild dependence of the DNA DSB induction on the quality of the incoming radiation, thus leading to a reported relative biological effectiveness (RBE) values for DSB induction usually not much higher than one (*11, 13, 18, 20, 22, 25*). However, DSB yields and RBE values for ion irradiation are higher, compared to fraction of activity released (FAR) assays, when DNA fragmentation in a number of fragment size intervals is taken into account in the analysis (*11, 13, 14, 18*), indicating a non-random induction of DSB.

Monte Carlo simulations performed with the PARTRAC (PARticle TRACks) code have demonstrated that the production of DSB by radiations of different qualities can be further investigated (*26–30*). In previous work (*31–36*) we have performed simulations with different radiation qualities and showed that in some high-LET cases, the number of fragments smaller than 1 kbp account for about half of the total number. Our results also have shown that the total DSB yield is considerably higher for high-LET than for low-LET radiations (and higher than usually measured), and that quantitatively most of the radiation quality dependence of the fragmentation spectrum comes from the production of (very) small fragments.

In this study we have used the PARTRAC code to again show that the underestimation of the number of small fragments, in PFGE experiments, is due to an incorrect analysis of the data. In these experiments the different gel segments, after the electrophoresis, contain DNA fragments of length belonging to different length bins (since the shorter the fragment, the larger the migration distance in the gel); the measured quantity is the DNA mass in each gel segment, from which the number of corresponding DNA fragments is estimated. This analysis is generally done by using the mid-value of that length bin, i.e., the arithmetic mean of the lower limit and the upper limit of the bin and the DNA mass divided by this mid-length gives the number of fragments in the bin. Thus, from the measured DNA mass distribution one can compute the DNA fragment number distribution. However, if the distribution of fragment lengths inside a bin is not symmetrical around the mid-length, this procedure leads to an incorrect evaluation of the number of fragments, as explained in the Materials and Methods section. This is particularly problematic in the estimation of the number of small fragments. In PARTRAC simulations the number of fragments in each length bin is simply counted, and it is not obtained by averaging within fragment length bins. Therefore, the simulation of the DNA fragmentation, after irradiation with a given ion beam, allows a more accurate comparison and evaluation of the number of fragments obtained in PFGE experiments.

In these studies, we have simulated the irradiation of human cells with four different nitrogen-ion beams, differing in the specific energy and therefore in the LET with the four LET values of 80, 125, 175 and 225 keV/μm, respectively. The LET values were chose to allow direct comparison with the experimental fragmentation spectra obtained by Höglund and Stenerlöw (*37*) and the corresponding DSB yield determination (*18*). To complete the comparison with that study, we also simulated irradiation with γ rays. We found that the agreement between the PARTRAC and the experimental DNA mass distributions is excellent in all cases. In particular, we found agreement for the mass fractions, for all LET values, in the lowest size interval, 0–48 kbp. However, comparison of DNA fragment distributions as LET increased revealed that the number of fragments in the simulations were much larger than the one computed from the experimental data. We show here that this inadequate experimental data analysis leads to a considerable underestimation of the RBE for DSB production and an incorrect decreasing trend with increasing LET in ref. (*18*).

MATERIALS AND METHODS

The Biophysical Monte Carlo Code PARTRAC

The biophysical simulation code PARTRAC is based on an ''event by event'' description of radiation track structure in liquid water at the nanometer level, combined with an atom-by-atom simulation of the biological target. The current version of the code, structured in modules, can simulate the transport and interaction of electrons, photons, protons, He ions and heavier ions. Further details on the physical models embedded in PARTRAC can be found elsewhere (*28, 29*). The DNA target model was designed to represent, on an atomic basis, the whole genome (about 6 Gbp) of a diploid human fibroblast in interphase. The simulated target presents six levels of DNA organization (deoxynucleotide pair, double helix, nucleosome, chromatin fiber, chromatin fiber loops and chromosome territories). In the present study, a model cell of a human fibroblast cell was irradiated with a parallel beam of nitrogen ions and with a parallel beam of γ rays. In particular the simulations with nitrogen ions have been performed with a source positioned near the cell and generating parallel beams with LET values 80, 125, 175 or 225 keV/μm. The LET values and the doses (150 Gy with γ rays and 64, 100, 140 and 200 Gy, respectively, for nitrogen beams) are those reported in ref. (*37*). Particle starting points, energy and directions of secondary electrons were used as input data of the secondary electron module. The simulated yields of radiation induced DNA strand breaks were determined by superimposition of the track structure pattern of inelastic events on the DNA target model. Concerning indirect effects, ionized water molecules were assumed to dissociate under different schemes as reported in ref. (*28*). Diffusion and reaction processes of the different chemical species were simulated by the chemical module embedded in the PARTRAC code. The production of DNA single-strand breaks, accounting for both direct (i.e., direct energy deposition) and indirect (radical-mediated) effects, has been described in detail previously (*28*). Here it suffices to say that a DSB is assumed to occur when two strand breaks are found on opposite strands within 10 base pairs.

The fragmentation analysis started with the output data set of the PARTRAC effect module, containing the genomic positions of DSBs due to irradiation with different doses. A fragment is the portion of double-stranded DNA between two adjacent DSBs or between a DSB and a chromosome end. The genomic distance between the two adjacent DSBs or between the DSB and the chromosome end defines the fragment length. It is clear from this assumption that each DSB increases the number of DNA fragments by 1. Further and comprehensive details on the physics and DNA target models embedded in the code can be found in a review by Friedland *et al*. (*30*). After irradiation simulations, the code outputs containing the different DNA damage data were analyzed in terms of fragments spectra for different fragment size intervals. We emphasize that we are considering only the initial DNA damage, since the rejoining process is inhibited; therefore, our PARTRAC simulations do not consider repair. Each point in the figures below, was obtained by running the code 10 times for each dose for nitrogen ions and γ rays; we found that this number of runs was sufficient, since more simulations did not change the results significantly. Errors for each point of the simulation data are standard deviations of the results obtained in the performed runs.

Data Analysis

The PARTRAC DNA damage module contains the genomic positions of DSB. From these data one can obtains the number of DNA fragments, and the length of each of them, by calculating the distance between adjacent breaks or between a break and a chromosome end. The fragment number spectrum is then determined, assigning each fragment accordingly to the proper size interval. The mass distribution is derived by multiplying each fragment by its length (obviously proportional to its molecular weight), summing all these products and dividing the result by the width of the interval. The size intervals that we have chosen are the same as used by Höglund and Stenerlöw (*37*), to compare the distributions; the intervals are given by the following values, in kbp: 0–48, 48–97, 97–145, 145–225, 225–375, 375–680, 680–930, 930-1110, 1110–3500, 3500–5750.

We note here that the evaluation of the experimental distributions follow reversed paths in the simulations and in the experimental procedures. We summarize the two kinds of analyses here. In a PARTRAC simulation the number $N_{i,th}$ of DNA fragments in the ith size interval is obtained directly. If m_j is the mass of the jth fragment belonging to that interval, then the total DNA mass in the ith size interval is given by

$$M^T_{i,th} = \sum_{j=1}^{N_{i,th}} m_j. \tag{1}$$

We note that the average mass of the fragments in the ith interval, given by

$$M_{i,av} = \frac{1}{N_{i,th}} \sum_{j=1}^{N_{i,th}} m_j = \frac{M^T_{i,th}}{N_{i,th}}, \tag{2}$$

is in general different from the mid-range value M_i; as specified before, this value is the arithmetic mean of the interval limits, i.e., $M_i = (1/2)(M_{i1} + M_{i1})$, where M_{i1} and M_{i1} are the lower and upper limit, respectively. In contrast, with gel electrophoresis one measures the amount of DNA in each gel segment, and therefore the mass distribution is directly determined. Therefore, if $M^T_{i,exp}$ is the measured DNA mass in the ith gel segment, the corresponding number of fragments $N_{i,\mathrm{exp}}$ is determined by

$$N_{i,exp} = \frac{M^T_{i,exp}}{M_i}, \tag{3}$$

where M_i, again, is the mid-range value in the ith interval. It should be clear that in principle this is only an approximation. To illustrate the difference let us suppose that the experimental and the theoretical masses in the ith segment, $M^T_{i,th}$ and $M^T_{i,exp}$, are identical. Then, if the exact number of fragments is $N_{i,\mathrm{th}}$, then the ratio of the approximated value of the experimental number of fragments, $N_{i,\mathrm{exp}}$, to the actual one, is given by

$$\frac{N_{i,exp}}{N_{i,th}} = \frac{M^T_{i,exp}}{M_i N_{i,th}} = \frac{M^T_{i,th}}{M_i N_{i,th}} = \frac{M_{i,av} N_{i,th}}{M_i N_{i,th}} = \frac{M_{i,av}}{M_i}, \tag{4}$$

where use has been made of Eqs. (2) and (3).

In ref. (*37*) the plots refer to the mass fraction distributions: the plotted value corresponding to the ith gel segment is

$$g_{i,exp} = \frac{M^T_{i,exp}}{M_g \Delta M_i}, \tag{5}$$

where M_g is the total mass of the genome, and ΔM_t is the width of the segment, i.e., $(M_{t2} - M_{i1})$. Then, the distributions of the mass fraction are actually plotted, but we can call them mass distributions without risk of confusion. Combining Eqs. (3) and (5), the experimental number of fragments $N_{i,\mathrm{exp}}$ is obtained by the reported value $g_{i,\mathrm{exp}}$ by

$$N_{i,exp} = \frac{g_{i,exp} M_g \Delta M_i}{M_i}. \tag{6}$$

RESULTS

We present here the PARTRAC results for the DNA fragment number spectra and the DNA mass distributions for the four nitrogen ion beams specified in the previous section, equal to those studied experimentally in ref. (*37*). In that work, together with the plots of the DNA mass distributions for the nitrogen beams, the analogous distributions obtained after irradiation with ^{60}Co γ rays are shown. Before proceeding with the description of the results, we explain how the data are presented. Since the plots in ref. (*37*) give the mass distributions through the values $g_{i,\mathrm{exp}}$ as explained in Eq. (5), we have conformed to this description also for the PARTRAC data. The experimental $g_{i,\mathrm{exp}}$, redrawn in our graphs, have been obtained from the plots of ref. (*37*). To make the comparison between experimental and PARTRAC fragment spectra, we obtained the experimental values $N_{i,\mathrm{exp}}$ through Eq. (6). We emphasize that this procedure is explicitly stated in ref. [(*37*; see Eq. (2)], although plots of fragment spectra are not provided in that paper.

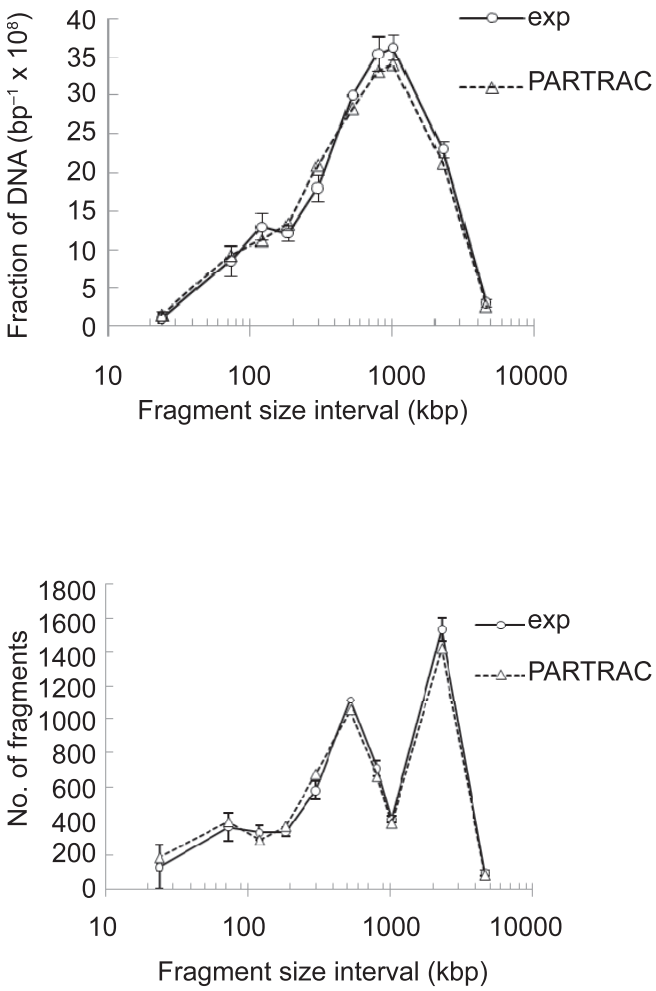

FIG. 1. Initial DNA mass distribution (upper panel) and initial DNA fragment spectrum (lower panel) plotted as a function of fragment size after irradiation with 150 Gy of ^{60}Co γ rays: comparison between experimental and PARTRAC data. In this figure and in Figs. 2–5 we have adopted the following common notations: in the x-axis each size is positioned at the size corresponding to the mid-range value of the corresponding size interval; errors for the experimental data are taken from ref. (*37*), while errors for the PARTRAC data are standard deviations of the results obtained in the performed runs (however, in all cases these standard deviations are contained within the symbol size).

We begin by first making the comparisons with the γ rays reference case; in Fig. 1 we plot the DNA mass distributions and the DNA fragment spectra after irradiation with photons, comparing the PARTRAC simulations and the experimental determinations. There is clear agreement between simulation and experimental data on both graphs. Similar comparisons are made in Figs. 2–5 for the nitrogen beams: 80 keV/μm (64 Gy), 125 keV/μm (100 Gy), 175 keV/μm (140 Gy) and 225 keV/μm (200 Gy), respectively.

The comparison between experimental and PARTRAC data shows that for all mass distributions the agreement appears reasonable. In addition, for the fragment spectra, the agreement is also good for all size intervals except the smallest one, 0–48 kbp. In this size interval [$i = 1$ in Eqs. (1–6)] the PARTRAC number of fragments $N_{1,th}$ is much larger than the experimental number $N_{1,\mathrm{exp}}$. Furthermore, Eq. (4) suggests that the average mass $M_{1,av}$ is much smaller than the mid-range mass $M_1 = 24$ kbp (please note, that the fragment masses can be indicated by their length). In Table 1 we give the value of the average fragment size in the smallest size interval for the four nitrogen beams as computed by PARTRAC using Eq. (2).

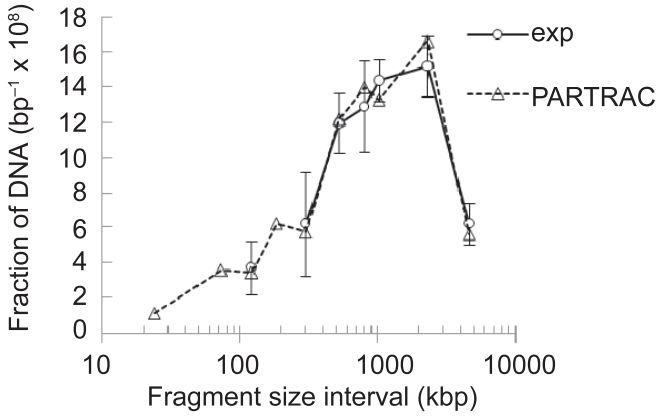

FIG. 2. Initial DNA mass distribution (upper panel) and initial DNA fragment spectrum (lower panel) plotted as a function of fragment size after irradiation with 64 Gy of nitrogen ions with LET equal to 80 keV/μm: comparison between experimental and PARTRAC data.

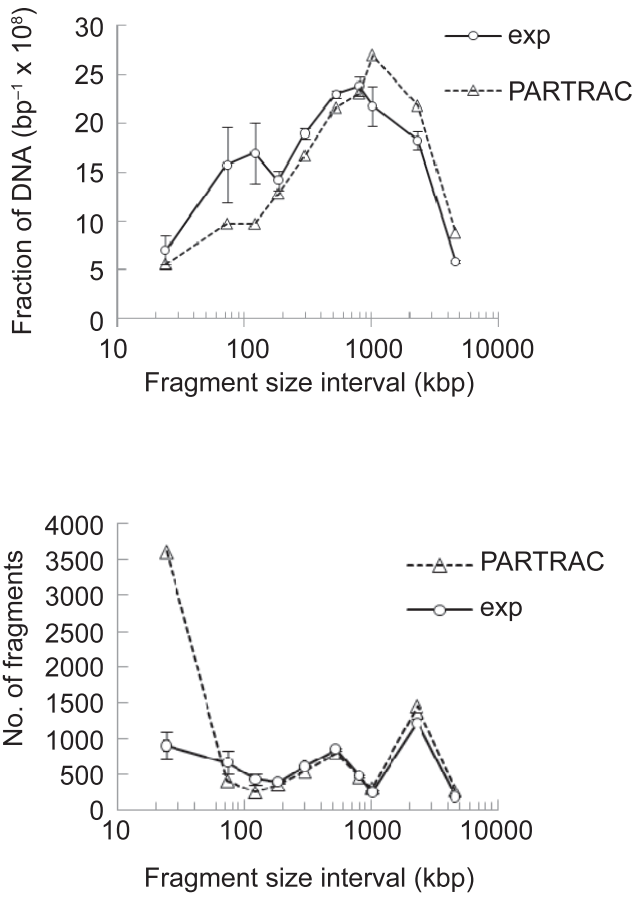

FIG. 3. Initial DNA mass distribution (upper panel) and initial DNA fragment spectrum (lower panel) plotted as a function of fragment size after irradiation with 100 Gy of nitrogen ions with LET equal to 125 keV/μm: comparison between experimental and PARTRAC data.

In Fig. 6 we plot the PARTRAC fragment number spectrum for the nitrogen beam of 125 keV/μm (in this case the data are plotted in the form of a distribution, i.e., with each number divided by the width of the corresponding bin) in the first size interval, 0–48 kbp, with a much finer binning within that interval. The two arrows in the plot denote the mid-range value, 24 kbp, and the average mass, which is about 6 kbp. We do not show analogous plots for the other nitrogen beams, but we refer to Table 1 for the average fragment lengths.

The large difference in the number of fragments in the first size interval between the experimental evaluation and the PARTRAC computation results in a considerable difference in the total number of fragments, and therefore in the DSB yield. Figure 7 shows the experimental yields (squares surrounded by circles) and the PARTRAC yields (triangles) as a function of LET, for the three LET values of

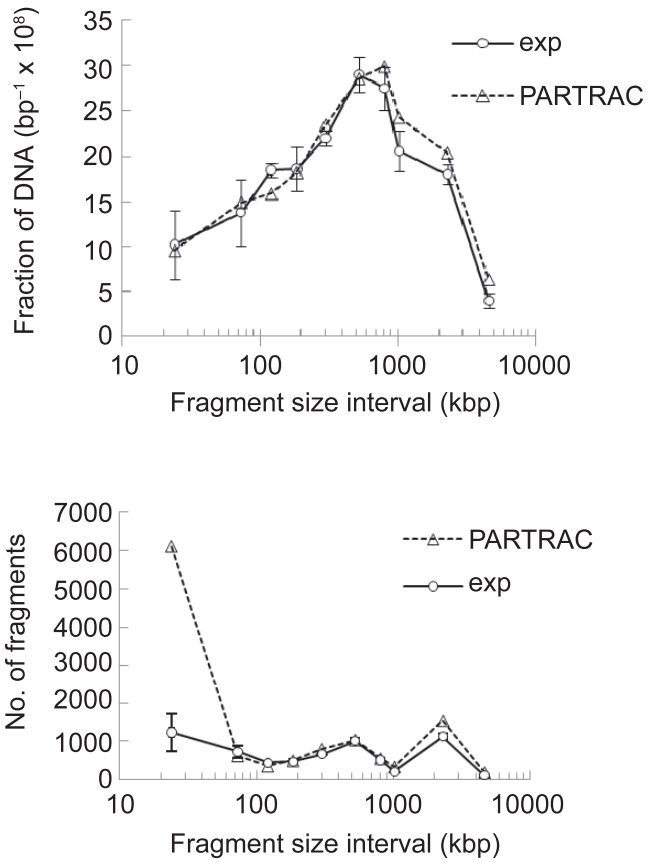

FIG. 4. Initial DNA mass distribution (upper panel) and initial DNA fragment spectrum (lower panel) plotted as a function of fragment size after irradiation with 140 Gy of nitrogen ions with LET equal to 175 keV/μm: comparison between experimental and PARTRAC data.

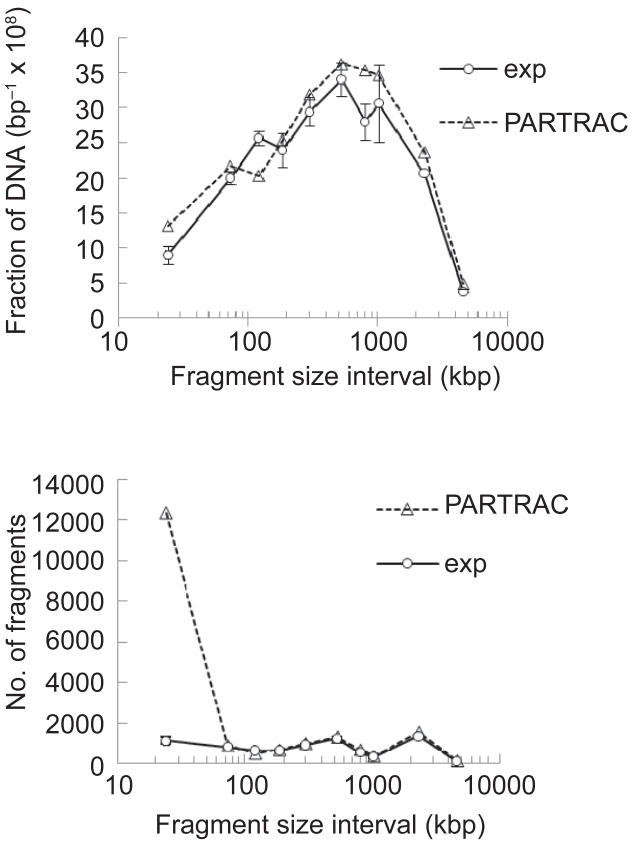

FIG. 5. Initial DNA mass distribution (upper panel) and initial DNA fragment spectrum (lower panel) plotted as a function of fragment size after irradiation with 200 Gy of nitrogen ions with LET equal to 225 keV/μm: comparison between experimental and PARTRAC data.

the nitrogen beams for which the experimental total number of fragments is available (based on the mass distribution as explained above). The γ-rays case is plotted at the LET value equal to 0.2 keV/μm (the LET value usually associated to γ rays, corresponding to an average LET value of the secondary electrons). While the experimental and simulated data for γ rays are essentially equal, differences for the three nitrogen ion beams are clearly evident. In Fig. 7 a third set of values (crosses) shows the re-evaluated experimental yields, obtained by computing the experimental number of fragments in the first size interval, with Eq. (6), with the mid-range value $M_1 = 24$ kbp substituted by the average mass value evaluated by PARTRAC, and given in Table 1. As expected, these corrected experimental yields are practically equivalent to the PARTRAC yields, since the agreement between the experimental and theoretical mass distributions is quite good. The residual difference for the highest LET value can be ascribed to the difference in the first point of the mass distributions (Fig. 5, upper panel); a difference that is not present for the other two nitrogen LET values (Figs. 3 and 4, upper panels) considered in Fig. 7. The PARTRAC RBE values for DSB production for the three nitrogen beams of Fig. 7 are 2.30, 2.35 and 2.68 for the nitrogen beam with LET equal to 125, 175 and 225 keV/μm, respectively, and thus show a slight upward trend with increasing LET.

DISCUSSION AND CONCLUSIONS

The results of the PARTRAC simulations presented in this article were compared with the experimental measurements previously published (*18, 37*). We found good agreement for the DNA mass distributions, however fragment spectra analysis revealed that for the nitrogen beams especially for the points corresponding to the

TABLE 1
Average Fragment Size in the Fragment Size Range 0–48 kbp for the Four Nitrogen Ion Beams as Computed by PARTRAC

LET (keV/μm)	Average size in the size range 0–48 kbp
80	16.6 kbp
125	6.0 kbp
175	4.8 kbp
225	2.4 kbp

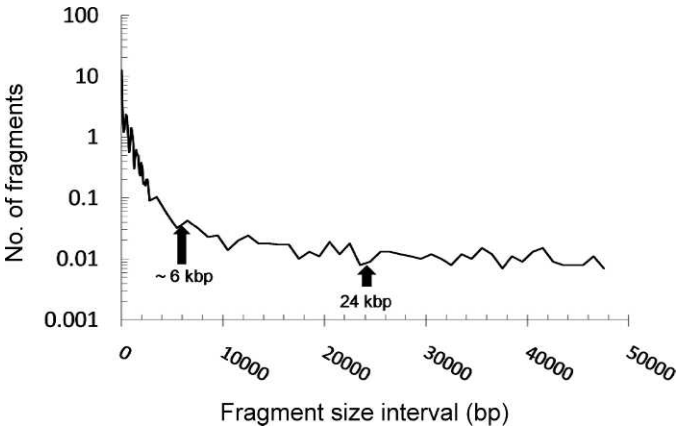

FIG. 6. Initial DNA fragmentation distribution, in the size interval 0–48 kbp, after irradiation with 100 Gy of nitrogen ions with LET equal to 125 keV/μm, as obtained with the PARTRAC code. The distribution is obtained from the spectrum dividing by the width of the corresponding bin, and using a quite fine binning within the interval. Vertical arrows indicate the mid-range fragment length that has been used in experimental data calculations (24 kbp) and the average fragment length obtained from the PARTRAC data (6 kbp).

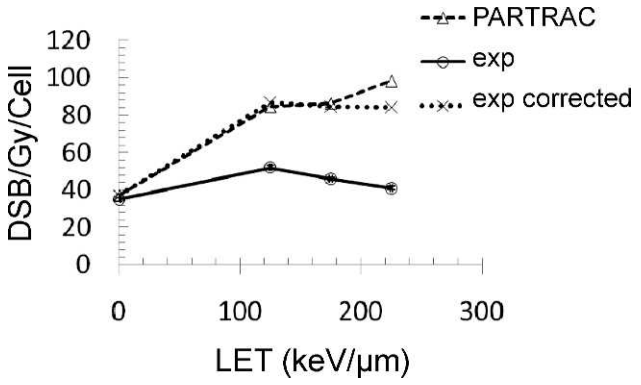

FIG. 7. Comparison between curves of DSB/Gy/cell, i.e., the yield, as a function of LET: experimental data (continuous line) (*37*) and PARTRAC data (dashed line with Δ symbols). The dotted line with × symbols is the experimental curve corrected using the average fragment length obtained for the smallest fragment size interval, for each LET value, with the PARTRAC code.

smallest size interval, 0–48 kbp data was widely divergent. This disagreement with the experimental evaluation was due to an assumption of the mid-range length, 24 kbp, instead of the average length. With re-evaluation of the experimental results, using a computed average length in the 0–48 kbp size interval, results in an RBE for DSB production of about 2.3 for the nitrogen beams with LET values 125, 175 and 225 keV/μm.

Clearly, procedure of using mid-range values instead of average lengths was incorrect and has strong influence at low-molecular weights while at high-molecular weights the width of the interval is small with respect to its mid-range, so that, even if the fragment distribution is not symmetrical around the mid-range, the error introduced is small. In the case of the γ-rays fragment spectrum, the disagreement for the smallest size interval was not present, due both to the smaller number of small fragments produced and to a more symmetrical distribution inside the smallest size interval, 0–48 kbp.

The data strongly suggest that in this size interval the nitrogen beams produce a nonflat fragment distribution as a result of the complex structure of the fragment distribution at small scale induced by high-LET irradiation. This structure is completely lost if the distribution is substituted by one symmetrically centered on the mid-range value, 24 kbp, as was assumed in the evaluation of the number of fragments from the mass fraction by Höglund and Stenerlöw (*37*).

The repair efficiency is assumed to be affected mainly by the DSB clusters (*9*), clustered DSB being likely a frequent source of unrejoined DSB. Therefore, an underestimation of the number of small fragments could result in an even more marked underestimation of the number of residual DSB. This in turn will lead to an underestimation of the RBE for residual DSB for radiation of different qualities. As a consequence, the inclusion of DSB associated with small DNA fragments is of crucial importance in the construction of a mechanistic model for the relationship between initial damage, damage processing and late cellular effects. We note that recently the ''Local Effect Model'' of Scholz and collaborators has been updated with a version that gives special consideration to the importance of clustered DSB (*38*). In that model clustered DSB are those that occur, in number of two or more in the same ''giant loop'' (*39*) of the chromatin organization. Therefore, in that model the cell response at a given dose depends on the relative numbers of loops with clustered and isolated DSB and takes into account the role of DSB clusters in cell survival.

Another potentially important issue in modeling DNA damage is that of heat labile sites. Investigators have found that with a cold lysis protocol (*40*) the number of DSB induced by low-LET radiation is about 30% less. In our study we compare experiments done with standard (hot lysis) protocols, and the initial damage in the simulations includes conversion of heat labile sites to DSB. The probability of DSB induction in our PARTRAC simulations therefore reflects the experimental setup of hot lysis, and the DSB yields therefore correspond to this condition. We note that heat labile sites are found to be more related to indirect effects (*41*); thus, the large production of small fragments by high-LET ions, mostly due to direct effects, is largely independent from them. Obviously, an explicit consideration of heat labile sites would be necessary for comparisons with experiments done in cold lysis protocols, and it may be of importance for the dynamics of DNA damage response (*42*). Our present study does not deal with these cases.

A detailed knowledge of the DSB distribution, and of its dependence on track structure and on chromatin conformation, is only the first step in understanding the mechanisms that lead to cellular end points such as cell death. Building a

realistic model able to explain the paths responsible for different cell fates would require, in addition, a quantitative description of the processes playing a role in the repair machinery. Since these processes depend on the characteristics of the initial radiation induced damage, a proper knowledge of these properties is a prerequisite for the determination of cellular response to radiation damage. Recent advances in the PARTRAC code has been extended, with the non-homologous end-joining in DSB repair (*42–44*), also modeled in ref. (*45*) other studies are now considering radiation induced signal release [theoretically and experimentally investigated in ref. (*46–48*)], that are possibly responsible for the bystander effects (*49, 50*). The validation process of these important model upgrades requires that a satisfactory agreement be found with the data on rejoining kinetics and on the cellular end points. This process is still in its infancy (*42–44, 50*) and its successful accomplishment could give the PARTRAC code a powerful predictive power for radiation effects. Towards this end, we believe that an exact determination of the initial damage, and the help that current Monte Carlo code can offer can help overcome current experimental limitations and be a very useful tool to investigators.

ACKNOWLEDGMENTS

The authors are very much indebted to Pavel Kundrát for a careful reading of the manuscript and for his suggestions. This work was partially funded by EU (EC Contract FP6- 36465, ''NOTE'', EC Contracts FP7-249689, ''DOREMI'' and 269553 ''EpiRadBio'').

Received: May 2, 2012; accepted: December 18, 2012; published online: May 6, 2013

REFERENCES

1. Suzuki M, Watanabe M, Kanai T, Kase Y, Yatagai F, Kato T, et al. LET dependence of cell death, mutation induction and chromatin damage in human cells irradiated with accelerated carbon ions. Adv Space Res 1996; 18:127–36.
2. Belli M, Cera F, Cherubini R, Dalla Vecchia M, Haque AMI, Ianzini F, et al. RBE-LET relationships for cell inactivation and mutation induced by low energy protons in V79 cells: further results at the LNL facility. Int J Radiat Biol 1998; 74:501–9.
3. Anderson RM, Marsden SJ, Wright EG, Khadim MA, Goodhead DT, Griffin CS. Complex chromosome aberrations in peripheral blood lymphocytes as a potential biomarker of exposure to high-LET α-particles. Int J Radiat Biol 2000; 76:31–42.
4. Belloni F, Bettega D, Calzolari P, Cherubini R, Massariello P, Tallone L. Inactivation cross sections for mammalian cells exposed to charged particles: A phenomenological approach. Radiat Prot Dosim 2002; 99:109–202.
5. George K, Durante M, Wu H, Willingham V, Cucinotta FA. In vivo and in vitro measurements of complex-type chromosomal exchanges induced by heavy ions. Adv Space Res 2003; 31: 1525–35.
6. Durante M, George K, Gialanella G, Grossi G, La Tessa C, Manti L, et al. Cytogenetic effects of high-energy iron ions: dependence on shielding thickness and material. Radiat Res 2005; 164:571–6.
7. Lee R, Nasonova E, Ritter S. Chromosome aberrations yields and apoptosis in human lymphocites irradiated with Fe-ions of differing LET. Adv Space Res 2005; 35:268–75.
8. Bettega D, Calzolari P, Doneda L, Durante M, Tallone L. Early and delayed reproductive death in human cells exposed to high energy iron ion beams. Adv Space Res 2005; 35:280–5.
9. Goodhead DT. Initial events in the cellular effects of ionising radiations: clustered damage in DNA. Int J Radiat Biol 1994; 65:7–17.
10. Holley WR, Chatterjee A. Clusters of DNA damage induced by ionizing radiation:formation of short DNA fragments. I. Theoretical modeling. Radiat Res 1996; 145:188–99.
11. Löbrich M, Cooper PK, Rydberg B. Non-random distribution of DNA double-strand breaks induced by particle irradiation. Int J Radiat Biol 1996; 70:493–503.
12. Rydberg B. Clusters of DNA damage induced by ionizing radiation: Formation of short DNA fragments. II. Experimental detection. Radiat Res 1996; 145:200–9.
13. Newman HC, Prise KM, Folkard M, Michael BD. DNA double-strand break distributions in X-ray and α-particle irradiated V79 cells: evidence for non-random breakage. Int J Radiat Biol 1997; 71:347–63.
14. Prise KM, Ahnström G, Belli M, Carlsson J, Frankenberg D, Kiefer J, et al. A review of dsb induction data for varying quality radiation. Int J Radiat Biol 1998; 74:173–84.
15. Rydberg B, Holley WR, Mian IS, Chatterjee A. Chromatin conformation in living cells: support for a zig-zag model of the 30 nanometer chromatin fiber. J Mol Biol 1998; 284:71–84.
16. Frankenberg D, Brede HJ, Schrewe UJ, Steinmetz C, Frankenberg-Schwager M, Kasten G, et al. Induction of DNA double-strand breaks by ^{1}H and ^{4}He ions in primary human skin fibroblasts in the LET range of 8 to 124 keV μm^{-1}. Radiat Res 1999; 151:540–9.
17. Sachs RK, Ponomarev AL, Hahnfeldt PJ, Hlatky LR. Locations of radiation-produced DNA double strand breaks along chromosomes: a stochastic cluster process formalism. Math Biosc 1999; 159:165–87.
18. Höglund E, Blomquist E, Carlsson J, Stenerlöw B. DNA damage induced by radiation of different linear energy transfer: initial fragmentation. Int J Radiat Biol 2000; 76:539–47.
19. Ponomarev AL, Sachs RK. Radiation breakage of DNA: a model based on random-walk chromatin structure. J Math Biol 2001; 43:356–76.
20. Belli M, Cherubini R, Dalla Vecchia M, Dini V, Esposito G, Moschini G, et al. DNA fragmentation in V79 cells irradiated with light ions as measured by PFGE. I. Experimental results. Int J Radiat Biol 2002; 78:475–82.
21. Stenerlöw B, Höglund E. Rejoining of double-stranded DNA-fragments studied in different size-intervals. Int J Radiat Biol 2002; 78:1–7.
22. Belli M, Campa A, Dini V, Esposito G, Furusawa Y, Simone G, et al. DNA fragmentation induced in human fibroblasts by accelerated ^{56}Fe ions of differing energies. Radiat Res 2006; 165:713–20.
23. Ponomarev AL, Belli M, Hahnfeldt PJ, Hlatky L, Sachs RK, Cucinotta FA. A robust procedure for removing background damage in assays of radiation-induced DNA fragment distributions. Radiat Res 2006; 166:908–16.
24. Ponomarev AL, Cucinotta FA. Chromatin loops are responsible for higher counts of small DNA fragments induced by high-LET radiation, while chromosomal domains do not affect the fragment sizes. Int J Radiat Biol 2006; 82:293–305.
25. Karlsson KM, Stenerlöw B. Focus formation of DNA repair proteins in normal and repair-deficient cells irradiated with high-LET ions. Radiat Res 2004; 161:517–527.
26. Friedland W, Jacob P, Paretzke HG, Stork J. Monte Carlo simulation of the production of short DNA fragments by low-linear energy transfer radiation using higher-order DNA models. Radiat Res 1998; 150:170–82.
27. Friedland W, Jacob P, Paretzke HG, Merzagora M, Ottolenghi A.

Simulation of DNA fragment distributions after irradiation with photons. Radiat Environ Biophys 1999; 38:39–47.

28. Friedland W, Jacob P, Bernhardt P, Paretzke HG, Dingfelder M. Simulation of DNA damage after proton irradiation. Radiat Res 2003; 159:401–10.
29. Friedland W, Jacob P, Paretzke HG, Ottolenghi A, Ballarini F, Liotta M. Simulation of light ion induced DNA damage patterns. Radiat Prot Dosim 2006; 122:116–20.
30. Friedland W, Dingfelder M, Kundrát P, Jacob P. Track structures, DNA targets and radiation effects in the biophysical Monte Carlo simulation code PARTRAC. Mutat Res 2011; 71:28–40.
31. Campa A, Ballarini F, Belli M, Cherubini R, Dini V, Esposito G, et al. DNA DSB induced in human cells by charged particles and gamma rays: experimental results and theoretical approaches. Int J Radiat Biol 2005; 81:841–54.
32. Alloni D, Ballarini F, Belli M, Campa A, Esposito G, Friedland W, et al. Modeling of DNA fragmentation induced in human fibroblasts by ^{56}Fe ions. Adv Space Res 2007; 40:1401–07.
33. Campa A, Alloni D, Antonelli F, Ballerini F, Belli M, Dini V, et al. DNA fragmentation induced in human fibroblasts by ^{56}Fe ions: experimental data and Monte Carlo simulations. Radiat Res 2009; 171:438–45.
34. Alloni D, Campa A, Belli M, Esposito G, Facoetti A, Friedland W, et al. A Monte Carlo study of the radiation quality dependence of DNA spectra. Radiat Res 2010; 173:263–71.
35. Alloni D, Campa A, Belli M, Esposito G, Mariotti L, Liotta M, et al. Monte Carlo evaluation of dna fragmentation spectra induced by different radiation qualities. Radiat Prot Dosim 2011; 143:226–231.
36. Alloni D, Campa A, Friedland W, Mariotti L, Ottolenghi A. Track structure, radiation quality and initial radiobiological events: considerations based on the PARTRAC code experience. Int J Radiat Biol 2012; 88:77–86.
37. Höglund E, Stenerlöw B. Induction and rejoining of DNA double-strand breaks in normal human skin fibroblasts after exposure to radiation of different linear energy transfer: possible roles of track structure and chromatin organization. Radiat Res 2001; 155:818–25.
38. Friedrich T, Scholz U, Elsässer T, Durante M, Scholz M. Calculation of the biological effects of ion beams based on the microscopic spatial damage distribution pattern. Int J Radiat Biol 2012; 88:103–7.
39. Yokota H, van den Engh G, Hearst JE, Sachs RK, Trask BJ. Evidence for the organization of chromatin in megabase pair-sized loops arranged along a random walk path in the human G0/G1 interphase nucleus. J Cell Biol 1995; 130:1239–49.
40. Stenerlöw B, Karlsson KH, Cooper B, Rydberg B. Biochemical kinetics model of DSB repair and induction of gamma-H2AX foci by non-homologous end joining. Radiat Res 2003; 159:502–10.
41. Yokoya A, Cunniffe SMT, Stevens DL, O'Neill P. Effects of hydration on the induction of strand breaks, base lesions, and clustered damage in DNA films by α-radiation. J Phys Chem B 2003; 107:832–7.
42. Friedland W, Jacob P, Kundrát P. Stochastic simulation of DNA double-strand break repair by non-homologous end joining based on track structure calculations. Radiat Res 2010; 173:677–88.
43. Friedland W, Kundrát P, Jacob P. Stochastic modelling of DSB repair after photon and ion irradiation. Int J Radiat Biol 2012; 88:129–36.
44. Friedland W, Jacob P, Kundrát P. Mechanistic simulation of radiation damage to DNA and its repair: on the track towards systems radiation biology modelling. Radiat Prot Dosim 2011; 143:542–8.
45. Cucinotta FA, Pluth JM, Anderson JA, Harper JV, O'Neill P. Biochemical kinetics model of DSB repair and induction of gamma-H2AX foci by non-homologous end joining. Radiat Res 2008; 169:214–22.
46. Mariotti L, Facoetti A, Bertolotti A, Nano R, Pasi F, Ottolenghi A. Effects of ionizing radiation on cell-to-cell communication. Radiat Res 2010; 174:280–289.
47. Mariotti L, Facoetti A, Bertolotti A, Ranza E, Alloni D, Ottolenghi A. Radiation induced perturbation of cell-to-cell signaling and communication. Radiat Prot Dosim 2011; 143:294–300.
48. Mariotti L, Bertolotti A, Ranza E, Babini G, Ottolenghi A. Investigation of the mechanisms underpinning IL-6 cytokine release in bystander phenomena: the roles of radiation dose, radiation quality and specific ROS/RNS scavengers. Int J Radiat Biol. 2012, 88:751–762.
49. Friedland W, Kundrát P, Jacob P. Track structure calculations on hypothetical subcellular targets for the release of cell-killing signals in bystander experiments with medium transfer. Radiat Prot Dosim 2011; 143:325–9.
50. Kundrát P, Friedland W. Track structure calculations on targets responsible of signal release in bystander experiments with transfer of irradiated cell conditioned medium. Int J Radiat Biol 2012; 88:98–102.